International Journal of Pharmaceutics 627 (2022) 122261

Contents lists available at ScienceDirect

International Journal of Pharmaceutics

journal homepage: www.elsevier.com/locate/ijpharm

PET study of intravitreal adalimumab pharmacokinetics in a uveitis rat model

Xurxo García-Otero [a,b,c,1], Cristina Mondelo-García [d,e,1], Enrique Bandín-Vilar [d,e,1], Noemí Gómez-Lado [c,f], Jesús Silva-Rodríguez [b], David Rey-Bretal [b], M. Victoria Otero-Espinar [g], Alfredo Adan [h], Miguel González-Barcia [d,e], Pablo Aguiar [b,c,*], Francisco J. Otero-Espinar [a,i,j,*], Anxo Fernández-Ferreiro [d,e,*]

[a] Pharmacology, Pharmacy and Pharmaceutical Technology Department, Faculty of Pharmacy, University of Santiago de Compostela (USC), 15705 Santiago de Compostela, Spain
[b] Molecular Imaging Biomarkers and Nuclear Medicine Department, Health Research Institute of Santiago de Compostela (IDIS), 15706 Santiago de Compostela, Spain
[c] Molecular Imaging Biomarkers and Pharmacokinetic Modelling (MIBIOPHARM), Centre for Research in Molecular Medicine and Chronic Diseases (CIMUS), University of Santiago de Compostela (USC), 15782 Santiago de Compostela, Spain
[d] Clinical Pharmacology Group, University Clinical Hospital, Health Research Institute of Santiago de Compostela (IDIS), 15706 Santiago de Compostela, Spain
[e] Pharmacy Department, University Clinical Hospital of Santiago de Compostela (SERGAS), 15706 Santiago de Compostela, Spain
[f] Preclinical Imaging Facility, Experimental Biomedicine Centre (CEBEGA), University of Santiago de Compostela (USC), 15782 Santiago de Compostela, Spain
[g] Statistics, Mathematical Analysis and Optimisation Department, Faculty of Mathematics, University of Santiago de Compostela (USC), and Galician Center for Mathematical Research and Technology (CITMAga), 15782 Santiago de Compostela, Spain
[h] Department of Ophthalmology, Hospital Clinic of Barcelona, 08036 Barcelona, Spain
[i] Paraquasil Group, University Clinical Hospital, Health Research Institute of Santiago de Compostela (IDIS), 15706 Santiago de Compostela, Spain
[j] Institute of Materials, iMATUS, University of Santiago de Compostela (USC), 15782 Santiago de Compostela, Spain

ARTICLE INFO

Keywords:
Adalimumab
Anti-TNFα
Pharmacokinetics
Molecular imaging
Positron Emission Tomography
Endotoxin-induced uveitis

ABSTRACT

Adalimumab is an anti-TNFα drug approved for uveitis treatment by subcutaneous injection. This administration route exposes patients to systemic adverse effects and makes difficult to obtain therapeutic drug concentrations in the site of action due to the anatomical and physiological barriers of the eye. These inconveniences could be avoided by intravitreal injection. The aim of this study is to evaluate the pharmacokinetic profile and the biodistribution of the intravitreal administration of ^{89}Zr-adalimumab in a uveitis rat model using PET imaging. Adalimumab was radiolabelled to ^{89}Zr with a maximum specific activity of 10 MBq/mg. Four μL containing ≃1.74 MBq of ^{89}Zr-labelled adalimumab were injected into the vitreous. A microPET acquisition was carried out immediately after the injection and at different time points through a 10-day study and blood samples were obtained through the tail vein. Radiolabelling was successfully performed with a radiochemical purity after ultrafiltration of 99.69 %. The antibody ocular pharmacokinetics followed a one-compartment model, showing an intraocular elimination half-life of 15.57 h for healthy rats and 33.64 h for rats with uveitis, implying that ^{89}Zr-adalimumab remains around two times longer in rats with the disease compared to healthy ones. However, blood concentration half-life had similar values in both groups. In conclusion, this study shows for the first time the ocular and blood pharmacokinetic analysis of adalimumab in a uveitis model in rats.

1. Introduction

Uveitis includes multiple heterogeneous clinical entities of ocular diseases which are characterized by the inflammation of the uveal tissue, involving iris, ciliary body and choroid (Bonnet and Brézin, 2020; Tsirouki et al., 2018). With regard to epidemiology, there is a wide variability in reported data with an estimated incidence between 17 and 52 per 100 000 of population per year, and a prevalence of 38–714 cases per 100 000 of population (Acharya et al., 2013; Hwang et al., 2012; Tsirouki et al., 2018). In spite of its rarity, this eye disease is an

* Corresponding authors.
E-mail addresses: pablo.aguiar.fernandez@sergas.es (P. Aguiar), francisco.otero@usc.es (F.J. Otero-Espinar), anxordes@gmail.com (A. Fernández-Ferreiro).
[1] The authors contributed equally.

https://doi.org/10.1016/j.ijpharm.2022.122261
Received 22 July 2022; Received in revised form 17 September 2022; Accepted 28 September 2022
Available online 5 October 2022

important cause of ocular morbidity, being the third leading cause of blindness in developed countries (Fanlo et al., 2019; Hart et al., 2019).

Non-infectious uveitis requires in many cases corticosteroids and immunosuppressive therapy, which can effectively control the inflammation. Depending on the location and severity of the inflammation, topical eye drops may not be enough and systemic oral administration has to be performed (Shahab et al., 2019). Long-term treatment with these agents can cause severe side effects, such as renal and hepatic toxicity, hypertension, and hematologic abnormalities (Hamam et al., 2016). Tumour necrosis factor alpha (TNFα) inhibitors constitute an option in these patients due to its promising mechanism of action (Murray and Sivaraj, 2005; Robertson et al., 2003). The presence of TNFα in the serum and aqueous humour of subjects with active uveitis has been demonstrated in clinical and preclinical studies (Hamam et al., 2016; Nakamura et al., 1994; Pérez-Guijo et al., 2004; Santos Lacomba et al., 2001; Sugita et al., 2007). Specifically, it has been reported that TNFα may induce the expression of adhesion molecules, chemokines and cytokines which are involved in inflammation. Consequently, inhibition of TNFα produce results in suppression of infiltrating macrophages, hence preventing tissue destruction (Hamam et al., 2016; Murray and Sivaraj, 2005; Robertson et al., 2003).

At present, there is already an approved anti-TNFα drug (adalimumab) for the treatment of uveitis that has shown promising results ("Humira," 2018). However, its subcutaneous administration entails two major inconveniences. On the one hand, the patient is exposed to adverse effects associated with the systemic exposition to the drug and, on the other hand, it is difficult to obtain therapeutic drug concentrations in the site of action due to the anatomical and physiological barriers of the eye, which is relatively isolated from the systemic circulation by the tight blood-retinal barrier (Castro-Balado et al., 2020; Sánchez-López et al., 2017; Varela-Fernández et al., 2020). To circumvent these limitations, a clinical trial has been carried out in order to compare intravitreal vs subcutaneous administration of adalimumab in uveitis patients, but without reporting results (American University of Beirut Medical Center, 2016). Furthermore, intravitreal administration has been explored in other ocular diseases such as choroidal neovascularization secondary or diabetic macular retinopathy (Hospital Universitari Vall d'Hebron Research Institute, 2012; Rafic Hariri University Hospital, 2011).

In the clinical setting, the dose and frequency of adalimumab administration are based on concentrations obtained from plasma and not on intravitreal pharmacokinetic studies due to the invasiveness of collecting vitreous samples. In this sense, the study of intravitreal adalimumab pharmacokinetics in humans should be preceded by a detailed characterization of its pharmacokinetics in preclinical models of uveitis providing information on drug concentration not only in the blood, but more importantly at the site of action (eye) and different organs and tissues of the whole body. In this regard, intravitreal pharmacokinetic preclinical studies are usually carried out collecting vitreous samples over time on animals sacrificed at different time points. According to the 3Rs principles in animal experimentation ("The Principles of Humane Experimental Technique," 1960), these studies can be efficiently performed using Positron Emission Tomography (PET), which represents a promising non-invasive imaging tool for the evaluation of the pharmacokinetic and biodistribution of antibodies. PET pharmacokinetic studies provide images showing the *in vivo* targeting and off-targeting of the antibodies and a follow-up over time in the same animal, avoiding the collection of multiple vitreous samples over time and other tedious procedures, and drastically reducing the number of animals needed. Furthermore, these studies provide quantitative information in real time, enabling to estimate the pharmacokinetic profile by carrying out longitudinal studies with several measures of each animal over time (Fernández-Ferreiro et al., 2017). However, this technique requires previous steps that can be challenging, mainly those related to the radiolabelling of the antibodies. On this basis, Zirconium-89 (^{89}Zr) is the PET radionuclide of choice for the radiolabelling of antibodies because of its long half-life (3.3 days), which is favourable for evaluating the *in vivo* distribution during several days, and its chemical properties suitable for the radiolabelling of antibodies using different chelators. To date, although multiple antibodies have been radiolabelled in order to conduct PET pharmacokinetic studies in different clinical areas, mainly in oncology (Verel et al., 2003), the radiolabelling of adalimumab has not been still described.

The aim of this study is to evaluate the pharmacokinetic profile and the biodistribution of the intravitreal administration of ^{89}Zr-adalimumab in a uveitis rat model using PET imaging.

2. Material and methods

2.1. Conjugation, radiolabelling and quality control

The radiolabelling of adalimumab has been carried out according to the procedures previously developed by Verel *et al.* for other monoclonal antibodies (Verel et al., 2003), which consist of two phases:

2.1.1. Adalimumab conjugation

Adalimumab (Imraldi®; Biogen S.L., Madrid, Spain) was purified against MilliQ water using Amicon® Ultra-2 mL (NMWL 30 kDa) centrifugal filters (Merck®Millipore®, Burlington, Massachussets, USA) to remove other excipients of the commercial product. Once the purified antibody was obtained, a 2-fold molar excess of tetrafluorphenil-*N*-succinyldeferoxamine-B-Fe^{3+} (TFP-*N*-sucDf-Fe) (ABX®, Radeberg, Germany) was added in order to conjugate the molecule. Conjugation was carried out at 25 °C for 30 min in constant motion, adjusting the solution to pH 9.0–9.5 with 0.1 M Na_2CO_3. Once this time has elapsed, the pH was again reduced to pH 4.0–4.5 with 0.25 M H_2SO_4 and a 50-fold excess of 25 mg/mL EDTA (ethylenediaminetetraacetic acid) was added to trap the iron found in the TFP-*N*-sucDf-Fe molecule, and then, they were incubated at 30 °C for 30 min. Conjugated adalimumab was again purified adjusting the antibody concentration to the same as the commercial solution (50 mg/mL). Once the antibody conjugation was completed, the *N*-sucDf-adalimumab was stored at −80 °C to maintain it in optimal conditions.

2.1.2. Adalimumab radiolabelling

Prior to radiolabelling, adalimumab was kept at room temperature until completely thawed. The required amount of clinical grade ^{89}Zr-oxalate solution (BV cyclotron VU, PerkinElmer, Inc., Waltham, Massachusetts, USA) was collected with 1 M oxalic acid. To perform the proper labelling reaction, the pH was raised to a range of pH 4.0–4.5 with 2 M Na_2CO_3 and then HEPES buffer (4-(2-hydroxyethyl)-1-piperazineethanesulfonic acid) was added until a solution at pH 7 was obtained. Once the pH was achieved, the *N*-sucDf-adalimumab was added to the solution and incubated for 1.5 h at room temperature. Adalimumab was labelled with a maximum specific activity of 10 MBq/mg. Afterwards, an ultrafiltration with Amicon® Ultra-0.5 mL Centrifugal Filters, NMWL 100 kDa (Merck®Millipore®, Burlington, Massachusetts, USA) was carried out in order to concentrate and purify the solution.

2.1.3. Quality control

The adalimumab conjugation quality control was performed with a size-exclusion high-performance liquid chromatography (SE-HPLC) using an HPLC system (Agilent 1260 series; Agilent Technologies®, Santa Clara, CA, USA) to check whether antibodies aggregation and fragmentation processes occurred during conjugation, as well as to calculate the conjugation ratio between the *N*-sucDf and the adalimumab. An Agilent Bio *SEC*-5, 5 µm, 300 Å, 7.8 × 150 mm column was used with a flow rate of 0.7 mL/min, the mobile phase consisted of phosphate-buffered saline (PBS; pH 7.4). The UV-detector wavelengths were set to 220, 280 and 430 nm. The ratio of conjugated TFP-*N*-sucDf to the protein was determined by the antibody-bound versus unbound 430 nm signal of Fe^{3+} on SE-HPLC (Luaces-Rodríguez et al., 2020).

The radiochemical purity (RCP) of labelled adalimumab was evaluated by trichloroacetic acid (TCA) precipitation test. It was performed by mixing equal amounts of 1 % HSA (Human Serum Albumin) (Albunorm® 20 %, Octapharma®, Lachen, Switzerland) in PBS and 20 % trichloroacetic acid in MilliQ water, an aliquot of the labelled compound is added to this solution. The sample was centrifuged to separate the precipitate (protein fraction) from the supernatant, and the radioactivity in both fractions were measured by a well counter (Atomlab® Wipe Test Counter, Biodex®, New York, USA) to determine the RCP (Luaces-Rodríguez et al., 2020).

2.2. Endotoxin-induced uveitis model (EIU)

In vivo studies were carried out on male Sprague-Dawley rats with an average weight of 250 g supplied by the animal facility at the University of Santiago de Compostela (CEBEGA, Santiago de Compostela, Spain). The animals were kept in cages under controlled temperature (22 ± 1 °C) and humidity (60 ± 5 %), with day-night cycles regulated by artificial light (12/12 h) and feeding *ad libitum*. The animals were treated according to the ARVO statement for the use of animals in ophthalmic and vision research as well as the approved guidelines for laboratory animals ("Guide for the Care and Use of Laboratory Animals - NCBI Bookshelf," n.d.; "The Association for Research in Vision and Ophthalmology- Statement for the Use of Animals in Ophthalmic and Vision Research," n.d.). Experiments were approved by the Committee for Ethical Research of the Health Research Institute of Santiago de Compostela (IDIS) (15012/2021/001) and followed the Spanish and European Union (EU) rules (86/609/CEE, 2003/ 65/CE, 2010/63/EU, RD 1201/2005, and RD53/2013). Our study design consisted of a control group of healthy rats (n = 3; 6 eyes) and a uveitis group of endotoxin-induced uveitis (EIU) rats (n = 6, 12 eyes). EIU model has demonstrated being highly appropriate due to its reproducibility and its similar clinical changes to those appearing in human uveitis (Garg et al., 2021). This model was induced inoculating 1 mg/kg *Escherichia coli* lipopolysaccharide endotoxin (LPS) diluted in 0.1 mL balance salt solution (BSS) into the rat's right paw as previously performed by our group (García-Otero et al., 2021) and by other authors (da Silva et al., 2011; Girol et al., 2013).

2.3. Intravitreal administration of ^{89}Zr-adalimumab

Rats were kept in a veterinary gas chamber containing 3 % (v/v) isoflurane/oxygen (Baxter®, Deerfield, Illinois, USA). Once anaesthetized, rats were placed in a surface where they continued receiving anaesthesia with a face mask (2.5 % isoflurane/oxygen). Intravitreal injection was performed according to the procedure described in our previous articles (Fernández-Ferreiro et al., 2017; Luaces-Rodríguez et al., 2020). Topical anaesthetic eye drops (1 mg/mL tetracaine hydrochloride, 4 mg/mL oxybuprocaine Hydrochloride; Colircusí anestésico doble®, Alcon Healthcare, Texas, USA) were instilled in both eyes followed by mydriatic eye drops (10 mg/mL cyclopentolate hydrochloride; Colircusí Ciclopléjico®, Alcon Healthcare, Texas, USA) in order to visualize the eye fundus. The injection procedure was carried out 12 h after model induction by using a surgical microscope (Takagi OM-5 220–2; Takagi, Tokyo, Japan). A volume of 4 μL of the ^{89}Zr-labelled adalimumab was injected into the vitreous through pars plana using a NanoFil® syringe (WPI, Friedberg, Germany) attached to a 35 G needle. Concerning the activity of the radiolabelled compound, ≃ 1.74 MBq (≃ 0.17 mg of ^{89}Zr-adalimumab) was injected into each rat eye (≃ 3.48 MBq total activity injected per rat). Eyes with lens damage, or with significant bleeding when the intravitreal injection was made, were discarded from the study.

2.4. PET acquisition and image analysis

A preclinical PET/CT system (Albira model by Bruker Biospin, Billerica, Massachusetts, USA) was used to perform PET acquisitions immediately after intravitreal administration. Two-bed position of 10 min sequential acquisitions were carried out to include the whole body of rats. All animals were kept anaesthetized with 2.5 % isoflurane/oxygen through a face mask during the acquisition and the respiration frequency was continuously monitored. Each animal was scanned at different time points (0, 2, 4, 8, 12, 24, 36 h and every day from 2 to 10 days) following the same process to obtain the pharmacokinetic profile. Dynamic PET images were reconstructed using the maximum likelihood expectation maximization (MLEM) algorithm with 12 iterations and an image pixel size of 0.5 × 0.5 × 0.5 mm^3. All images were analysed using Amide's Medical Image Data Analysis Tool. Quantitative analysis was carried out on the different image frames by manually drawing ellipsoidal regions of interest (ROIs) of 12 × 12 × 12 mm (904 mm^3), significantly larger than the volume of whole rat eye in order to include all the radiotracer uptake of each eye (the contour of the radiotracer distribution is commonly blurred due to the limited spatial resolution of the PET scanners). The mean radiotracer concentration obtained from the first image frame after intravitreal administration was taken as reference, and the subsequent measures from the following frames were expressed as a percentage of this initial uptake. Additional ROIs (7 × 7 × 7 mm, 343 mm^3) were delineated in the heart, liver, spleen and cervical lymph nodes for each time. The mean radiotracer concentration derived from the different ROIs was corrected by the radioactive decay of the ^{89}Zr radioisotope (half-life of 3.3 days).

The standardized uptake value (SUV) was calculated as the mean uptake of ^{89}Zr-adalimumab normalized by the injected activity and the bodyweight of the animal, as shown in the following Equation (1).

$$SUV = \frac{measuredradioactivityconcentration(Bq/mL)}{injectedradioactivity(Bq)/bodyweight(Kg)} \quad (1)$$

Finally, a blood sample was obtained through the tail vein of each rat immediately after every PET acquisition while maintaining the anaesthesia. Specifically, two aliquots of a known volume (between 20 and 100 μL) were extracted and measured in a well counter (Atomlab® Wipe Test Counter, Biodex®, New York, USA). Measured activity from the blood samples was also corrected for the radioactive decay of ^{89}Zr. Total blood activity was calculated taking into account the theoretical rat blood volume calculated based on body weight using the expression: (Blood volume = 0.06 × Body weight + 0.77 (Lee and Blaufox, 1985)).

Finally, blood activity levels after intravitreal injection of ^{89}Zr-adalimumab were reported as the ^{89}Zr-adalimumab uptake value normalized by the injected activity and the bodyweight of the animal (Activity (%)). The scheme of the experimental design of the study is shown in Fig. 1.

2.5. Pharmacokinetic analysis

Compartmental data analyses were carried out using GraphPad Prism 8 v.8.2.1 software (GraphPad Software, San Diego, CA, USA) to calculate the pharmacokinetic parameters of the intravitreally injected radiolabelled adalimumab. One- and two-compartment models were used to fit the concentration vs time. Nonlinear regression methodology was used to fit experimental data. Nonlinear weighting method 1/Y^2 was used to fit the eye ^{89}Zr-adalimumab concentration decay. No weighting method was used for blood % activity fitting. To quantify the goodness of nonlinear fit, SE (Equation (2)), RMSE (Equation (3)) and Akaike method (AIC) parameters were used.

$$SE = \sqrt{\frac{\sum(residual^2)}{n-k}} \quad (2)$$

$$RMSE = \sqrt{\frac{\sum(residual^2)}{n-1}} \quad (3)$$

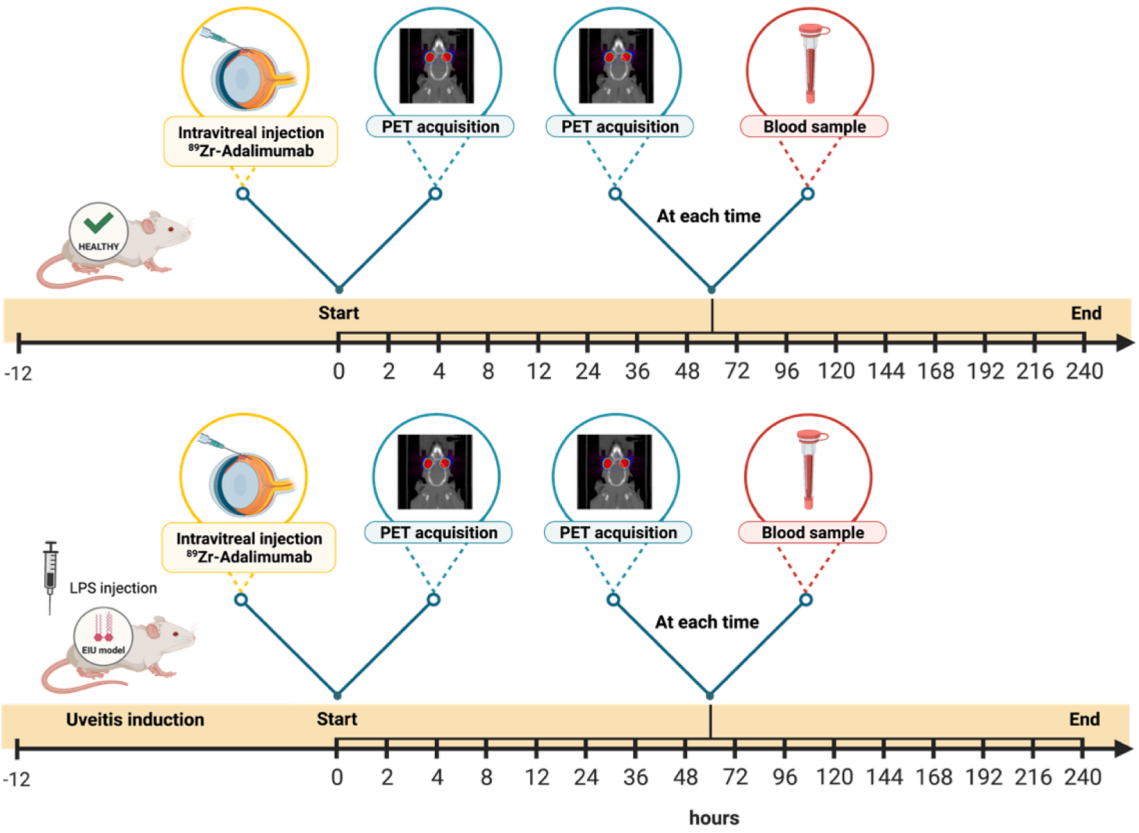

Fig. 1. Study timeline for both groups (Healthy and Uveitis group): EIU model induction, intravitreal injections of ^{89}Zr-adalimumab, PET acquisitions and blood sample collection. Created with BioRender.com.

where k is the number of fitted parameters by regression.

The compartmental analysis of ^{89}Zr-adalimumab distribution in eye was performed using models a) and b) of Fig. 2 and the Equations (5) and (8). In the case of blood distribution models b) and c) and Equations (9) and (13) were used:

Open intravitreal one-compartment model with a first order elimination kinetics from eye.

$$\frac{dX}{dt} = -\mathrm{k} \bullet \mathrm{X} \tag{4}$$

$$X = De^{-kt} \tag{5}$$

where D is the dose, X the adalimumab amount and k the elimination constant.

Open two-compartment model with intravitreal administration and linear elimination from peripheric compartment.

$$\frac{\mathrm{dX_1}}{\mathrm{dt}} = \mathrm{k_{21}X_2} - \mathrm{k_{12}} \bullet \mathrm{X_1} \tag{6}$$

$$\frac{dX_2}{dt} = k_{12}X_1 - k_{21} \bullet X_2 - k_{20} \bullet X_2 \tag{7}$$

$$X_1 = \frac{D(\beta - k_{12})}{\beta - \alpha}e^{-\alpha t} + \frac{D(k_{12} - \alpha)}{\beta - \alpha}e^{-\beta t} \tag{8}$$

$$X_2 = \frac{Dk_{12}}{\beta - \alpha}\left(e^{-\alpha t} - e^{-\beta t}\right) \tag{9}$$

where

$$\alpha + \beta = k_{12} + k_{21} + k_{20} \tag{10}$$

$$\alpha \bullet \beta = \mathrm{k_{12}} \bullet \mathrm{k_{21}} \tag{11}$$

D is the dose, X_1 is the adalimumab amount in the central compartment (eye) and X_2 the amount in the peripheric compartment. k_{12} and k_{21} are the distribution constant, k_{20} the elimination constant, and α and β the hybrid constant of two-compartment model.

Open one-compartment model with first order incorporation kinetic and linear elimination (blood).

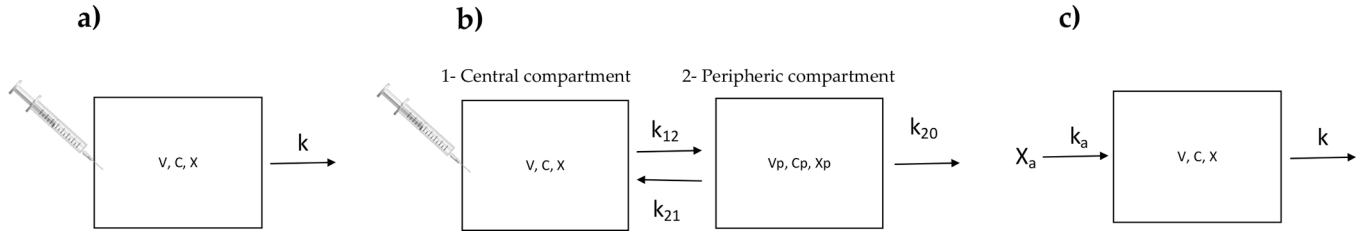

Fig. 2. Compartmental analysis of ^{89}Zr-adalimumab distribution. **a)** Open intravitreal one-compartment model with first order elimination kinetics from eye, **b)** Open two-compartment model with intravitreal administration and linear elimination from peripheric compartment and **c)** Open one-compartment model with first order incorporation kinetic and linear elimination (blood).

$$\frac{dX}{dt} = k_a X_a - k \bullet X \tag{12}$$

$$X = \frac{Dk_a}{k_a - k}\left(e^{-kt} - e^{-k_a t}\right) \tag{13}$$

where D is the dose, X_a is the adalimumab amount in the eyes, X the adalimumab amount in blood, k_a is the distribution constant from eyes to blood and k the elimination constant.

The curve of remaining radioactivity in the eye (%) versus time and curves of the SUV in blood, heart, liver, spleen and cervical lymph nodes in each rat versus time after intravitreal injection of ^{89}Zr-adalimumab were generated using GraphPad Prism 8 v.8.2.1 software (GraphPad Software, San Diego, CA, USA). Statistical analysis was performed to verify if there were significant differences between the Healthy and the Uveitis group. Two-tailed Mann-Whitney test and two-tailed parametric *t*-test were carried out for the different pharmacokinetic parameters, elimination and absorption constant (k and k_a), and also for the area under the curve (AUC_0^∞) and mean residence time (MRT), respectively. MRT gives information about the average time that adalimumab molecule remains in the eye or in the blood depending on the data. This parameter is calculated with the following Equation (14):

$$MRT = \frac{\int_0^\infty t \bullet C(t)dt}{\int_0^\infty C(t)dt} = \frac{AUMC_0^\infty}{AUC_0^\infty} \tag{14}$$

where C (t) is the concentration at each time t. The AUC_0^∞ and $AUMC_0^\infty$ were calculated using trapezoidal rules.

Since the volume of distribution (V) observed in rabbits and humans is similar to the vitreous anatomical volume, the same assumptions are made for rats (del Amo et al., 2015; del Amo and Urtti, 2015; Schmitt et al., 2019). Volume (V) value was calculated according to the experimental results obtained by Sha *et al.* (Sha and Kwong, 2006) and taking into account that the rats used in this study were 10 weeks old. The clearance (CL) can be calculated according to the following equation CL = k · V, where k corresponds to the rate elimination constant, and the vitreous anatomical volume (V) is 47 μL. The same distribution volume was used for both healthy and uveitis rats.

3. Results

3.1. Conjugation, radiolabelling and quality control

The conjugation result between the chelating agent (*N*-sucDf) and the antibody was 1.466 chelating groups per adalimumab molecule. The *N*-sucDf group percentage bound to the antibody that is available for ^{89}Zr chelation was 94.37 % for *N*-sucDf-adalimumab. The absence of adalimumab dimerization processes during conjugation was achieved, avoiding a loss of antibody activity in this step.

The result obtained for the radiolabelling efficiency of ^{89}Zr-adalimumab was 90.36 %. This radiolabelled compound was subjected to an ultrafiltration process in which a Radiochemical purity (RCP) of 99.69 % was obtained.

3.2. Pharmacokinetics after intravitreal administration

3.2.1. Ocular levels

The radioactive uptake of ^{89}Zr-adalimumab at different times through PET/CT images in the group of healthy rats and uveitis rats is shown in Fig. 3. It is possible to appreciate that the uptake in the eye declines as the study progresses in both groups. Nevertheless, there is a greater uptake at all times in the case of the Uveitis group except at the initial time, since it starts from the same activity. The information that can be obtained in these images is shown in more detail in Fig. 4.

As can be seen in Fig. 4, the percentage of remaining activity in the eye after intravitreal injection shows significant differences between healthy rats and uveitis rats. In Healthy group, there is a much more pronounced ocular elimination during the first timepoints post-injection compared to the Uveitis group. In contrast, in the Uveitis group, the antibody clearance occurs more slowly.

Fitting parameters of eye pharmacokinetic data to one- or two-compartment models are shown in Table 1. Both models had a well adjustment to the experimental concentrations with similar fit

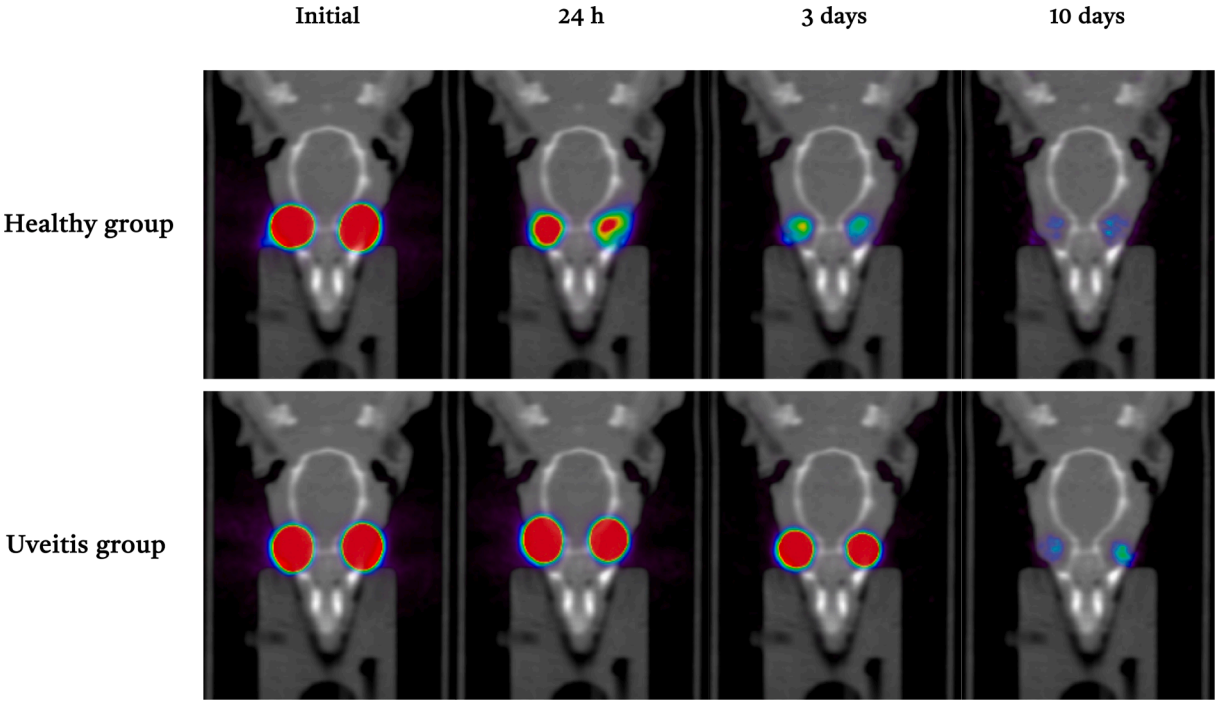

Fig. 3. Fused PET/CT images displayed in coronal plane showing rats head at different time points (initial, 24 h, 3 days and 10 days) following intravitreal administration of ^{89}Zr-adalimumab in both groups (Healthy and Uveitis). The colour scale represents the radioactive uptake of ^{89}Zr-adalimumab from lower (blue) to higher (red) intensity.

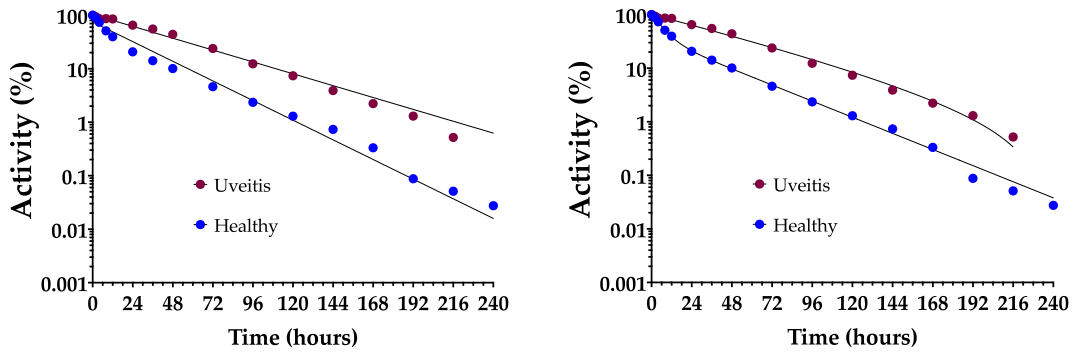

Fig. 4. Percentage of remaining radioactivity in the eye versus time after intravitreal injection of ^{89}Zr-adalimumab in both rat groups (Healthy n = 6 eyes and Uveitis n = 12 eyes). Filled dots (measured by PET) and error bars represent the mean ± SD of the observed values, whereas the solid lines represent the predicted values obtained by a one-compartment model (left, Equation (5)) and two-compartment model with intravitreal administration (right, Equation (8) central compartment).

Table 1
Results of the fitting of the eye ^{89}Zr-adalimumab concentration to the one-compartment model (Equation (5)) and two-compartment model with intravitreal administration (Equation (8) central compartment).

	Healthy group		Uveitis group	
Parameter	One-compartment model	Two-compartment model	One-compartment model	Two-compartment model
k	0.0445 h^{-1}		0.0206 h^{-1}	
alfa		0.0041 h^{-1}		0.0206 h^{-1}
beta		0.0566 h^{-1}		4.9x10^{-32}h^{-1}
k12		0.0525 h^{-1}		0.0194 h^{-1}
k21		0.0044 h^{-1}		5.3x10^{-32}h^{-1}
k20		0.0038 h^{-1}		0.0016 h^{-1}
Se	0.1538	0,1141	0.06728	0.07003
RMSE	0.1431	0.1041	0.06264	0.06264
AICs	−51.60	−58.07	−78,05	−73.69

parameter goodness. The two-compartment model has a very low k_{21} constant value in both groups suggesting that there is a minimal ^{89}Zr-adalimumab distribution from blood to the eye. As it can be seen in the semilogarithmic plots of Fig. 4, healthy animals show a slight two-compartment behaviour with the presence of a small initial distribution phase. However, this phase is not detected in the case of animals with uveitis. For this reason and for the fact that the k_{21} values are 12 times smaller than k_{12} the simplest one-compartment model can be selected to predict drug concentration.

Table 2 shows the results of some pharmacokinetic parameters concerning the elimination of intravitreal adalimumab. Half-life was 15.57 ± 2.64 h for healthy rats and 33.64 ± 6.69 h for uveitis rats, this implies that ^{89}Zr-adalimumab remains approximately-two times longer in diseased rats compared to healthy ones. The area under the ocular activity-time curve (AUC_0^∞) values was again higher for the Uveitis group (2540.66 ± 476.14 %·hours) than for the Healthy group (6624.59 ± 732.84 %·hours), this means that the adalimumab quantity inside the eye during the whole study is around three times higher in the diseased group. Finally, the mean residence time (MRT) was (56.07 ± 3.99 h) and (72.32 ± 10.86 h) for healthy rats and uveitis rats, respectively.

Table 2
Ocular pharmacokinetic parameters (mean ± SD) for the intraocular percentage of remaining activity using a one-compartment model after intravitreal injection of ^{89}Zr-adalimumab for both rat groups (Healthy n = 6 eyes and Uveitis n = 12 eyes).

Pharmacokinetic parameters	Healthy		Uveitis	
	Mean	SD	Mean	SD
k ($hours^{-1}$)	0.0445	0.007	0.0206	0.0083
$t_{1/2}$ (hours)	15.57	2.64	33.64	6.69
AUC_0^∞ (%·hour)	2540.66	476.14	6624.59	1397.37
MRT (hours)	56.07	3.99	72.32	10.86

A two-tailed Mann-Whitney test was performed to compare the elimination constant (k) of both groups showing significant differences ($\alpha < 0.05$) between them. In addition, a two-tailed parametric *t*-test was performed in order to compare the remaining adalimumab amount in the eye throughout the study (AUC_0^∞) and the residence time in the eye (MRT) of the two groups, confirming significant differences ($\alpha < 0.05$) in both parameters.

Regarding the ocular adalimumab clearance, it was 2.094 μL·h^{-1} for Healthy rats and 1.030 μL·h^{-1} for Uveitis rats (2 times faster in Healthy rats).

3.2.2. *Systemic distribution*

Fig. 5 shows the distribution of ^{89}Zr-adalimumab once it is eliminated from the eye into the systemic circulation. It is possible to observe that the uptake is increased sharply in heart, liver, spleen and cervical lymph nodes. In addition, two videos showing the whole-body distribution of ^{89}Zr-adalimumab in healthy and uveitis rats can be found as Supplementary material 1.

Fig. 6 represents the blood uptake values (Activity (%)) of ^{89}Zr-adalimumab for both groups during the entire study period. The rate of adalimumab distribution into the bloodstream was found to be higher in Healthy rats compared to Uveitis ones, while at longer times the antibody amount in blood is equalized.

As previously performed in the eye case, the blood ^{89}Zr-adalimumab distribution values were adjusted to a one- and two-compartment model (Table 3 and Fig. 6 solid lines). The values of SE, RMSE and AIC and the graphs in Fig. 6 show that healthy animals fit better the ^{89}Zr-adalimumab blood concentration to the two-compartment model. On the contrary, for the uveitis group, better fitting values were obtained for the one-compartment model. Additionally, the α and β hybrid constants estimated for two-compartment analysis show identical values. In consequence one-compartment model can be assumed for uveitis rats.

In order to compare the main pharmacokinetics parameters between Healthy and Uveitis groups, a non-compartmental analysis was made. The terminal half-life, maximum concentration (C_{max}) and time for maximum concentration (t_{max}) were estimated and the AUC_∞^0 and MRT were calculated as it is shown in Table 4. ^{89}Zr-adalimumab had a blood terminal half-life of 339 ± 96.90 h for the Healthy group and 295.93 ± 46.92 h for the Uveitis group. t_{max} were 12 ± 0 h for the healthy rats vs 84 ± 13.15 h for uveitis rats and C_{max} were 20.56 ± 3.61 % vs ± 21. 27 % respectively. The blood AUC_0^∞ values for both groups were 6026.15 ± 1727.21 (Healthy) and 5711.35 ± 1545.35 (Uveitis). MRT results were 172.97 ± 18.67 for the Healthy group and 175.18 ± 17.54 for the Uveitis group, respectively. The statistical differences between the pharmacokinetic parameters of the two groups were studied.

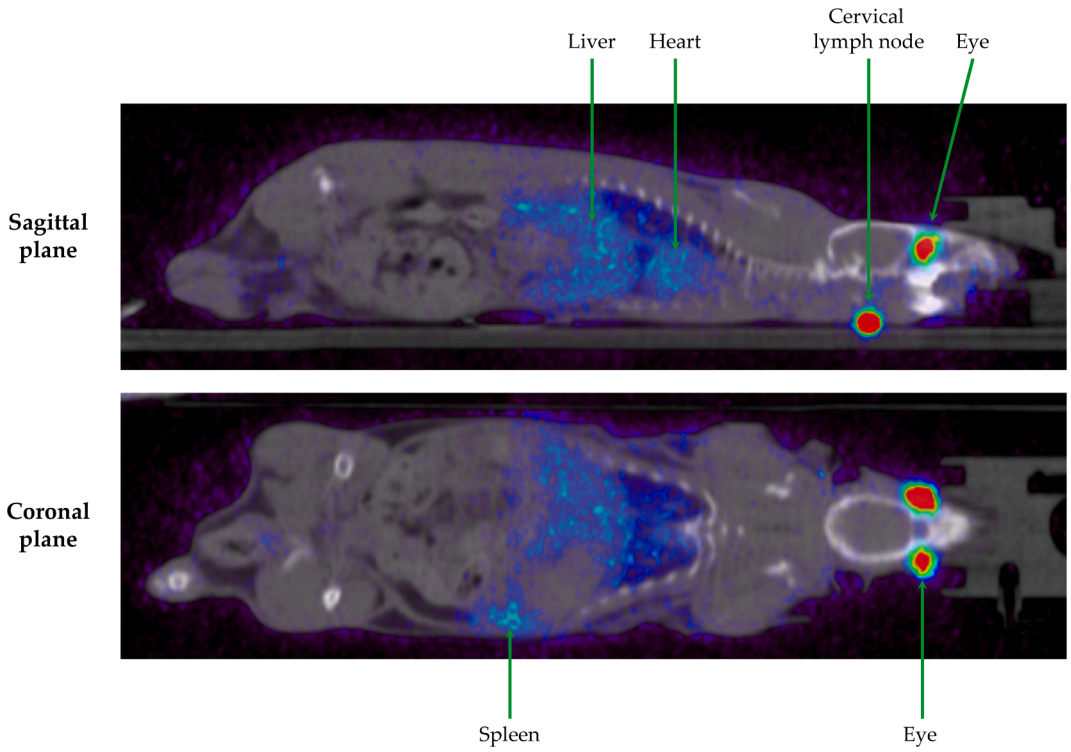

Fig. 5. Rat whole-body PET/CT images displayed in coronal plane (down) and sagittal plane (up) representing the ^{89}Zr-adalimumab distribution in the organs with the highest uptake. The colour scale represents the radioactive uptake of ^{89}Zr-adalimumab from lower (blue) to higher (red) intensity.

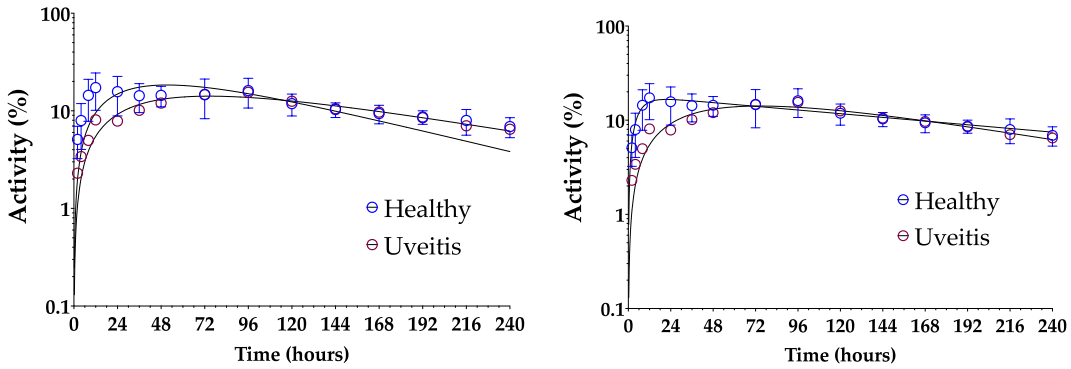

Fig. 6. Blood concentration (%) versus time after intravitreal injection of ^{89}Zr-adalimumab in both rat groups (Healthy and Uveitis). Unfilled dots (measured with well counter) and error bars represent the mean ± SD of the observed values, whereas the solid lines represent the predicted values obtained by the first-order absorption one-compartment model (left, Equation (4)) and two-compartment model (right, Equation (3) peripheric compartment).

The two-tailed Mann-Whitney test was performed on the terminal half-life showing no significant differences (ns). A two-tailed parametric *t*-test was carried out on C_{max}, AUC_0^{∞} and MRT. Significant differences were found in the t_{max} ($\alpha < 0.05$). Moreover, C_{max}, AUC_0^{∞} and MRT show no significant differences (ns) between both groups.

The pharmacokinetic results of the organs (heart, liver, spleen and cervical lymph nodes) were analysed, a first-order absorption one-compartment model was the best pharmacokinetics fit for these results. As shown in Fig. 7, in all the organs where there is uptake, it can be seen that the speed of adalimumab influx is faster in the Healthy rat group at short times. As time goes by, the curves overlap until they become equal in the last study stages for both groups, Healthy and Uveitis rats. During the study period, the elimination process of the monoclonal antibody is not clearly observed.

4. Discussion

To our knowledge, this is the first work addressing intravitreal pharmacokinetics of adalimumab. In this sense, regarding the ocular permanence of adalimumab, although the group of healthy animals shows a slight two-compartment behaviour, data obtained from PET analysis fits well with a one-compartment model for both Healthy and Uveitis groups. The one-compartment model providing significant differences in the k elimination constant from the eye, and subsequently in the time adalimumab remains in the eye (half-life of 15.57 ± 2.64 h for Healthy group and 33.64 ± 6.69 h for Uveitis group). These results seem to be in contradiction with the behaviour observed in a previous work comparing the pharmacokinetics of two radiopharmaceuticals, ^{18}F-NaF and ^{18}F-FDG (Fernández-Ferreiro et al., 2017). In this earlier work, an increase in ^{18}F-FDG clearance caused by inflammation was observed, while ^{18}F-NaF remained unchanged. The explanation for the possible causes of the observed increase in ^{18}F-FDG clearance in uveitis was the

Table 3
Results of the fitting of the eye ^{89}Zr-adalimumab blood concentration to the one-compartment model (Equation (13)) and two-compartment model with intravitreal administration (Equation (9) peripherical compartment).

	Healthy group		Uveitis group	
Parameter	One-compartment model	Two-compartment model	One-compartment model	Two-compartment model
k	0.0411 h^{-1}		0.006212 h^{-1}	
ka	0.0147 h^{-1}		0.02511 h^{-1}	
alfa		0.1957 h^{-1}		0.0127 h^{-1}
beta		0.0055 h^{-1}		0.0127 h^{-1}
k12		0.0414 h^{-1}		0.007 h^{-1}
k21		0.0265 h^{-1}		0.029 h^{-1}
k20		0.1397 h^{-1}		−0.009 h^{-1}
Se	4.604	1.094	2.439	2.378
RMSE	4.448	1.019	2.356	2.214
AICs	54.73	11.20	34.39	36.04

Table 4
Blood pharmacokinetic non-compartmental parameters (terminal half-life, t_{max}, C_{max}, AUC_0^∞, mean residence time (MRT)) (mean ± SD) for blood concentration data using a first-order absorption one-compartment model after intravitreal injection of ^{89}Zr-adalimumab in both rat groups (Healthy and Uveitis).

Pharmacokinetic parameters	Healthy		Uveitis	
	Mean	SD	Mean	SD
Terminal half-life (hours)	339	96.9	295.93	46.92
t_{max} (hours)	12	0	84	13.15
C_{max} (%)	20.56	3.61	21.27	6.54
AUC_0^∞ (%·hour)	6026.15	1727.21	5711.35	1545.35
MRT (hours)	172.97	18.67	175.18	17.54

increased permeability of blood-retinal barrier and the GLUT transporter.

However, the ability of the adalimumab to selectively bind to the tumour necrosis factor is well known. Thus, this result is consistent with the overproduction of TNFα from macrophages and other cytokines in the uveitis process, which activates dendritic cells, starting the inflammatory cascade in which Th1 cells and Th17 cells migrate and infiltrate to the blood-retinal barrier causing damage (Jang et al., 2021). This overproduction of TNFα was shown in a previous work of our group where rats with uveitis presented a higher presence of TNFα mRNA in the eye tissues than healthy rats (García-Otero et al., 2021). These measures of TNFα levels have also been carried out by other authors in the preclinical and clinical setting (Hamam et al., 2016; Nakamura et al., 1994). Due to this biochemical mechanism, adalimumab is specifically blocking the binding of human TNFα to the receptors in the Uveitis group. Since adalimumab binds to TNFα receptors located in the uvea, its ocular clearance will be diminished.

The results of the pharmacokinetic compartmental analysis in blood show a different behaviour between healthy and diseased animals. The activity vs time in healthy animals fits to a two-compartment model showing a rapid uptake of the antibody from the eye simultaneous to the tissue distribution process. However, in the case of animals with uveitis, the activity vs time fits better to a one-compartment model. This may be because the transfer process from the eye to the blood is much slower acting as a limiting step, so that the distribution process to the organs is not appreciated.

In order to compare the rate and magnitude of adalimumab transfer from the eye to the blood, a non-compartmental analysis was used. Regarding to this, our results provided similar blood terminal half-life between the Healthy (339.00 ± 96.90 h) and Uveitis groups (295.93 ± 46.92 h), as well as MRT (172.97 ± 18.67 h and 175.18 ± 17.54 h, respectively), but significant differences in the t_{max} between Healthy

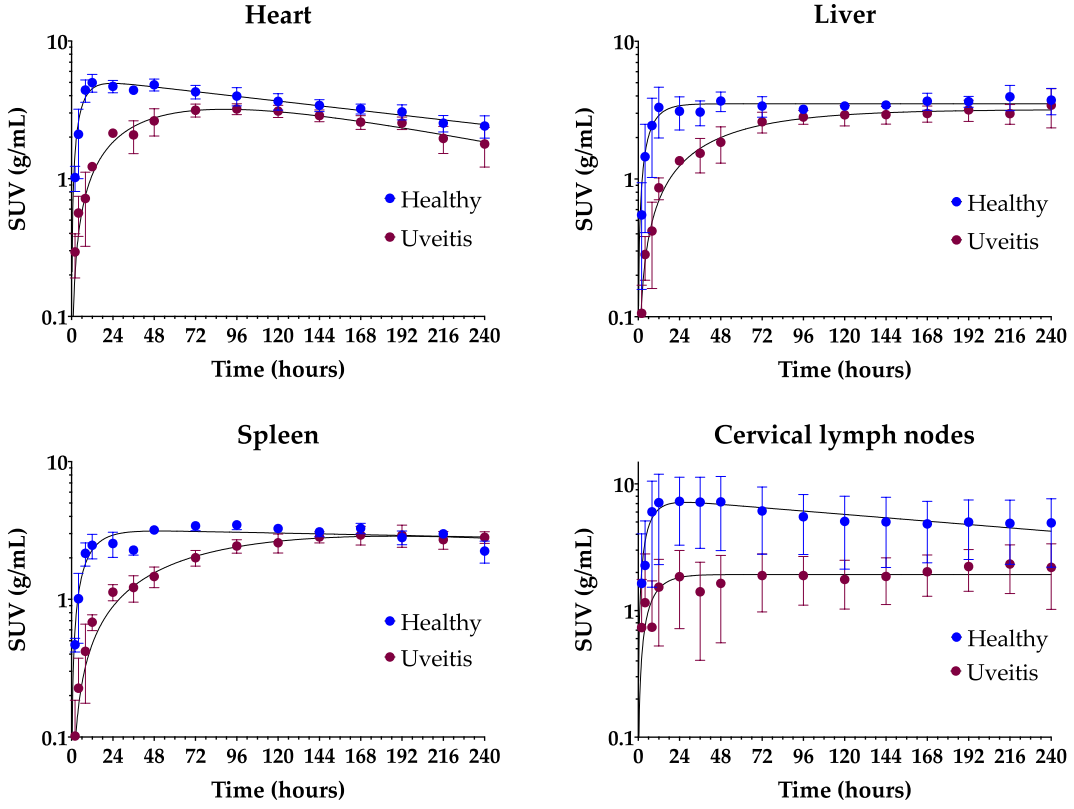

Fig. 7. Activity (SUV) in the different organs (heart, liver, spleen and cervical lymph nodes) versus time after intravitreal injection of ^{89}Zr-adalimumab in both rat groups (Healthy and Uveitis). Filled dots (measured by PET) and error bars represent the mean ± SD of the observed values, whereas the solid lines represent the predicted values obtained by a first-order absorption one-compartment model.

group and Uveitis group (12 ± 0.0 and 84 ± 13.15, respectively), probably due to the fact that, as can be observed in Fig. 6, up to 72 h the adalimumab amount in the blood of healthy rats is higher than that of uveitis rats. This could be caused by the binding between antibody and TNFα when the eyes are inflamed. Although ocular inflammation usually increases the permeability of ocular barriers and clearance of intravitreal drugs (Fernández-Ferreiro et al., 2017), our opposite results are due to the interaction between adalimumab and the TNFα (Horiuchi et al., 2010) present in the ocular cavity, which achieves increased values in uveitis as demonstrated in previous studies (García-Otero et al., 2021). After 72 h, blood values are equalized until the end of the study.

Intravitreal pharmacokinetic studies in patients are performed from the aqueous humour due to the impossibility of obtaining vitreous samples (García-Quintanilla et al., 2019). This procedure has also been carried out in the preclinical setting, specifically on animals sacrificed at different time points in order to obtain vitreous samples. In this sense, PET imaging has the advantage of avoiding invasive sampling and obtaining concentrations from the same animal over time, with the consequent decrease in the number of animals per study group (Fernández-Ferreiro et al., 2017). Additionally, PET methodology avoids the intrusiveness of the pharmacokinetic studies, which is very important taking into account the invasiveness of the intravitreal injection itself. PET imaging requires the use of radioactive derivatives which are stable over time. In this study, ^{89}Zr was selected because it allows to visualize the distribution of antibodies for up to 10 days due to its long half-life. In order to obtain radiolabelled adalimumab, deferoxamine was previously bound to this drug to act as a chelator of ^{89}Zr. As studied in previous works of our group (Luaces-Rodríguez et al., 2020), ^{89}Zr-labelled deferoxamine without monoclonal antibody has a completely different kinetic behaviour, the rate of elimination from both the vitreous cavity and blood is much faster (24 h) and that vitreous elimination is independent of the deferoxamine chelator, only the molecule has an influence.

The main limitation of our study regarding intravitreal pharmacokinetics is that all ocular cavities are measured together, including aqueous and vitreous humour, as well as surrounding tissues. However, this is partially counteracted by the fact that drug concentration declines with the same decay rate in the vitreous humour, aqueous humour and retina, as several authors state (Gadkar et al., 2015; Hutton-Smith et al., 2017). As well as other species, rats represent a good model for intravitreal pharmacokinetic studies (Sadeghi et al., 2021). However, comparison with humans should be cautiously made due to the anatomical and physiological ocular differences. With this regard, rats have a larger len and a simpler inner limiting membrane, which could be a poorer barrier to diffusion (Kern, 1997; Peynshaert et al., 2019), and around 50 μL of vitreous humour (Ahn et al., 2016), which is well below that volume in the human eye (4 mL). In addition, it is necessary to take into account that the stability of the metal complex formed between ^{89}Zr and the bifunctional chelate used (TFP-*N*-sucDf) was studied by Perk et al. who reported a small loss of ^{89}Zr from conjugate over a 7-day period (4.7 ± 0.5 %) (Perk et al., 2010), however, our study lasted 10 days so this loss could be slightly higher.

Regarding adalimumab pharmacokinetics outside the ocular cavity, interaction between the anti-TNFα that is removed from the eye and the major inflammatory agents is going to occur. The immune system is closely related to the lymphatic system, so an accumulation in the different lymph nodes close to the site of administration is expected, as can be confirmed by our results. In this sense, the highlighted area in the inferior part of the mandible (Fig. 5-sagittal plane) corresponds to the cervical lymph nodes, as described by Suami *et al.* (Suami and Scaglioni, 2017). The elimination process of adalimumab in the body cannot be clearly appreciated by observing the pharmacokinetic results of the main drug elimination organs. This is due to the fact that anti-TNFα has a large molecular weight (≃150 KDa), so filtration by the kidneys and elimination through urine is not possible, except under pathological conditions (Berdeja et al., 2016; Ryman and Meibohm, 2017). Thus, the main route of elimination occurs through intracellular catabolism by lysosomal degradation, transforming the monoclonal antibody into peptides and amino acids that can be re-used in the body for the *de novo* synthesis of proteins (Waldmann and Strober, 1969).

5. Conclusions

This study evaluates for the first time the pharmacokinetic profile of intravitreally injected adalimumab in a uveitis rat model, showing that this disease produces a major increase in the ocular permanence of this drug.

Funding.

This project has been partially funded by Instituto de Salud Carlos III (ISCIII) through the project PI20/00719 and co-funded by the European Union, Axencia Galega Innovación (Grupos de Potencial Crecimiento IN607B2020/11, Grupo de Referencia Competitiva ED431C2021/01 and ED431C2021/26 and Proyectos de Excelencia IN607D 2021/001) and Spanish Ministry of Science, Innovation and Universities (RTI2018-099597-B-100).

CRediT authorship contribution statement

Xurxo García-Otero: Investigation, Methodology, Formal analysis, Data curation, Writing – original draft, Visualization. **Cristina Mondelo-García:** Investigation, Validation, Writing – original draft, Visualization. **Enrique Bandín-Vilar:** Investigation, Validation. **Noemí Gómez-Lado:** Investigation, Methodology. **Jesús Silva-Rodríguez:** Methodology, Data curation. **David Rey-Bretal:** Investigation, Validation. **M. Victoria Otero-Espinar:** Methodology, Visualization, Writing – review & editing. **Alfredo Adan:** Conceptualization, Writing – review & editing. **Miguel González-Barcia:** Conceptualization, Resources, Writing – review & editing, Funding acquisition. **Pablo Aguiar:** Conceptualization, Resources, Writing – review & editing, Supervision, Project administration, Funding acquisition. **Francisco J. Otero-Espinar:** Conceptualization, Resources, Formal analysis, Data curation, Writing – review & editing, Visualization, Supervision, Project administration. **Anxo Fernández-Ferreiro:** Conceptualization, Resources, Writing – review & editing, Supervision, Project administration, Funding acquisition.

Declaration of Competing Interest

The authors declare that they have no known competing financial interests or personal relationships that could have appeared to influence the work reported in this paper.

Data availability

Data will be made available on request.

Acknowledgement

X. García-Otero is grateful to the IDIS (Health Research Institute of Santiago de Compostela) for financing his predoctoral research fellowship. C. Mondelo-García, E. Bandín-Vilar and A. Fernández-Ferreiro are grateful to the Carlos III Health Institute for financing their personnel contracts: JR20/00026, CM20/00135 and JR18/00014.

Appendix A. Supplementary material

Supplementary data to this article can be found online at https://doi.org/10.1016/j.ijpharm.2022.122261.

References

Acharya, N.R., Tham, V.M., Esterberg, E., Borkar, D.S., Parker, J.V., Vinoya, A.C., Uchida, A., 2013. Incidence and prevalence of uveitis: results from the Pacific Ocular Inflammation Study. JAMA Ophthalmol. 131, 1405–1412. https://doi.org/10.1001/jamaophthalmol.2013.4237.

Ahn, S.J., Hong, H.K., Na, Y.M., Park, S.J., Ahn, J., Oh, J., Chung, J.Y., Park, K.H., Woo, S.J., 2016. Use of Rabbit Eyes in Pharmacokinetic Studies of Intraocular Drugs. J. Vis. Exp. JoVE. https://doi.org/10.3791/53878.

American University of Beirut Medical Center, 2016. Efficacy of Intravitreal Adalimumab Compared to Subcutaneous Adalimumab in Patients With Non-infectious Uveitis (Clinical trial registration No. NCT02706704). clinicaltrials.gov.

Berdeja, J., Jagannath, S., Zonder, J., Badros, A., Kaufman, J.L., Manges, R., Gupta, M., Tendolkar, A., Lynch, M., Bleickardt, E., Paliwal, P., Vij, R., 2016. Pharmacokinetics and Safety of Elotuzumab Combined With Lenalidomide and Dexamethasone in Patients With Multiple Myeloma and Various Levels of Renal Impairment: Results of a Phase Ib Study. Clin. Lymphoma Myeloma Leuk. 16, 129–138. https://doi.org/10.1016/j.clml.2015.12.007.

Bonnet, C., Brézin, A., 2020. Uveitis: Diagnosis and work-up. J. Fr. Ophtalmol. 43, 145–151. https://doi.org/10.1016/j.jfo.2019.03.038.

Castro-Balado, A., Mondelo-García, C., Zarra-Ferro, I., Fernández-Ferreiro, A., 2020. New ophthalmic drug delivery systems. Farm. Hosp. Organo Of. Expresion Cient. Soc. Espanola Farm. Hosp. 44, 149–157. https://doi.org/10.7399/fh.11388.

da Silva, P.S., Girol, A.P., Oliani, S.M., 2011. Mast cells modulate the inflammatory process in endotoxin-induced uveitis. Mol. Vis. 17, 1310–1319.

del Amo, E.M., Urtti, A., 2015. Rabbit as an animal model for intravitreal pharmacokinetics: Clinical predictability and quality of the published data. Exp. Eye Res. 137, 111–124. https://doi.org/10.1016/j.exer.2015.05.003.

del Amo, E.M., Vellonen, K.-S., Kidron, H., Urtti, A., 2015. Intravitreal clearance and volume of distribution of compounds in rabbits: In silico prediction and pharmacokinetic simulations for drug development. Eur. J. Pharm. Biopharm. Special Issue on Ocular Drug Delivery 95, 215–226. https://doi.org/10.1016/j.ejpb.2015.01.003.

Fanlo, P., Heras, H., Espinosa, G., Adan, A., 2019. Complications and visual acuity of patients with uveitis: epidemiological study in a reference unit in northern Spain. Arch. Soc. Espanola Oftalmol. 94, 419–425. https://doi.org/10.1016/j.oftal.2019.05.005.

Fernández-Ferreiro, A., Luaces-Rodríguez, A., Aguiar, P., Pardo-Montero, J., González-Barcia, M., García-Varela, L., Herranz, M., Silva-Rodríguez, J., Gil-Martínez, M., Bermúdez, M.A., Vieites-Prado, A., Blanco-Méndez, J., Lamas, M.J., Gómez-Ulla, F., Ruibal, Á., Otero-Espinar, F.J., González, F., 2017. Preclinical PET Study of Intravitreal Injections. Invest. Ophthalmol. Vis. Sci. 58, 2843–2851. https://doi.org/10.1167/iovs.17-21812.

Gadkar, K., Pastuskovas, C.V., Le Couter, J.E., Elliott, J.M., Zhang, J., Lee, C.V., Sanowar, S., Fuh, G., Kim, H.S., Lombana, T.N., Spiess, C., Nakamura, M., Hass, P., Shatz, W., Meng, Y.G., Scheer, J.M., 2015. Design and Pharmacokinetic Characterization of Novel antibody formats for ocular therapeutics. Invest. Ophthalmol. Vis. Sci. 56, 5390–5400. https://doi.org/10.1167/iovs.15-17108.

García-Otero, X., Mondelo-García, C., González, F., Perez-Fernandez, R., Avila, L., Antúnez-López, J.R., González-Barcia, M., Adan, A., Aguiar, P., Otero-Espinar, F.J., Bermúdez, M.A., Fernández-Ferreiro, A., 2021. Anti-Inflammatory Effect of Tacrolimus/Hydroxypropyl-β-Cyclodextrin Eye Drops in an Endotoxin-Induced Uveitis Model. Pharmaceutics 13, 1737. https://doi.org/10.3390/pharmaceutics13101737.

García-Quintanilla, L., Luaces-Rodríguez, A., Gil-Martínez, M., Mondelo-García, C., Maroñas, O., Mangas-Sanjuan, V., González-Barcia, M., Zarra-Ferro, I., Aguiar, P., Otero-Espinar, F.J., Fernández-Ferreiro, A., 2019. Pharmacokinetics of Intravitreal Anti-VEGF Drugs in Age-Related Macular Degeneration. Pharmaceutics 11, E365. https://doi.org/10.3390/pharmaceutics11080365.

Garg, V., Nirmal, J., Riadi, Y., Kesharwani, P., Kohli, K., Jain, G.K., 2021. Amelioration of Endotoxin-Induced Uveitis in Rabbit by Topical Administration of Tacrolimus Proglycosome Nano-Vesicles. J. Pharm. Sci. 110, 871–875. https://doi.org/10.1016/j.xphs.2020.10.060.

Girol, A.P., Mimura, K.K.O., Drewes, C.C., Bolonheis, S.M., Solito, E., Farsky, S.H.P., Gil, C.D., Oliani, S.M., 2013. Anti-inflammatory mechanisms of the annexin A1 protein and its mimetic peptide Ac2-26 in models of ocular inflammation in vivo and in vitro. J. Immunol. Baltim. Md 1950 (190), 5689–5701. https://doi.org/10.4049/jimmunol.1202030.

Guide for the Care and Use of Laboratory Animals - NCBI Bookshelf [WWW Document], n.d. URL https://www.ncbi.nlm.nih.gov/books/NBK54050/ (accessed 1.17.22).

Hamam, R.N., Barikian, A.W., Antonios, R.S., Abdulaal, M.R., Alameddine, R.M., El Mollayess, G., Mansour, A.M., 2016. Intravitreal Adalimumab in Active Noninfectious Uveitis: a Pilot Study. Ocul. Immunol. Inflamm. 24, 319–326. https://doi.org/10.3109/09273948.2014.990041.

Hart, C.T., Zhu, E.Y., Crock, C., Rogers, S.L., Lim, L.L., 2019. Epidemiology of uveitis in urban Australia. Clin. Experiment. Ophthalmol. 47, 733–740. https://doi.org/10.1111/ceo.13517.

Horiuchi, T., Mitoma, H., Harashima, S., Tsukamoto, H., Shimoda, T., 2010. Transmembrane TNF-alpha: structure, function and interaction with anti-TNF agents. Rheumatol. Oxf. Engl. 49, 1215–1228. https://doi.org/10.1093/rheumatology/keq031.

Hospital Universitari Vall d'Hebron Research Institute, 2012. Open-label Clinical Trial to Evaluate Safety and Efficacy of Intravitreal Adalimumab in Patients With Choroidal Neovascularization Secondary to Age-related Macular Degeneration Non-responders to the Conventional Treatment With Ranibizumab (Clinical trial registration No. NCT01136252). clinicaltrials.gov.

Humira [WWW Document], 2018. . Eur. Med. Agency. URL https://www.ema.europa.eu/en/medicines/human/EPAR/humira (accessed 1.20.22).

Hutton-Smith, L.A., Gaffney, E.A., Byrne, H.M., Maini, P.K., Gadkar, K., Mazer, N.A., 2017. Ocular Pharmacokinetics of Therapeutic Antibodies Given by Intravitreal Injection: estimation of Retinal Permeabilities Using a 3-Compartment Semi-Mechanistic Model. Mol. Pharm. 14, 2690–2696. https://doi.org/10.1021/acs.molpharmaceut.7b00164.

Hwang, D.-K., Chou, Y.-J., Pu, C.-Y., Chou, P., 2012. Epidemiology of uveitis among the Chinese population in Taiwan: a population-based study. Ophthalmology 119, 2371–2376. https://doi.org/10.1016/j.ophtha.2012.05.026.

Jang, D., Lee, A.-H., Shin, H.-Y., Song, H.-R., Park, J.-H., Kang, T.-B., Lee, S.-R., Yang, S.-H., 2021. The Role of Tumor Necrosis Factor Alpha (TNF-α) in Autoimmune Disease and Current TNF-α Inhibitors in Therapeutics. Int. J. Mol. Sci. 22, 2719. https://doi.org/10.3390/ijms22052719.

Kern, T.J., 1997. Rabbit and rodent ophthalmology. Semin. Avian Exot. Pet Med. 6, 138–145. https://doi.org/10.1016/S1055-937X(97)80021-7.

Lee, H.B., Blaufox, M.D., 1985. Blood volume in the rat. J. Nucl. Med. Off. Publ. Soc. Nucl. Med. 26, 72–76.

Luaces-Rodríguez, A., Del Amo, E.M., Mondelo-García, C., Gómez-Lado, N., Gonzalez, F., Ruibal, Á., González-Barcia, M., Zarra-Ferro, I., Otero-Espinar, F.J., Fernández-Ferreiro, A., Aguiar, P., 2020. PET study of ocular and blood pharmacokinetics of intravitreal bevacizumab and aflibercept in rats. Eur. J. Pharm. Biopharm. Off. J. Arbeitsgemeinschaft Pharm. Verfahrenstechnik EV 154, 330–337. https://doi.org/10.1016/j.ejpb.2020.06.024.

Murray, P.I., Sivaraj, R.R., 2005. Anti-TNF-alpha therapy for uveitis: behçet and beyond. Eye Lond. Engl. 19, 831–833. https://doi.org/10.1038/sj.eye.6701792.

Nakamura, S., Yamakawa, T., Sugita, M., Kijima, M., Ishioka, M., Tanaka, S., Ohno, S., 1994. The role of tumor necrosis factor-alpha in the induction of experimental autoimmune uveoretinitis in mice. Invest. Ophthalmol. Vis. Sci. 35, 3884–3889.

Pérez-Guijo, V., Santos-Lacomba, M., Sánchez-Hernández, M., Castro-Villegas, M.D.C., Gallardo-Galera, J.M., Collantes-Estévez, E., 2004. Tumour necrosis factor-alpha levels in aqueous humour and serum from patients with uveitis: the involvement of HLA-B27. Curr. Med. Res. Opin. 20 (2), 155–157.

Perk, L.R., Vosjan, M.J.W.D., Visser, G.W.M., Budde, M., Jurek, P., Kiefer, G.E., van Dongen, G.A.M.S., 2010. p-Isothiocyanatobenzyl-desferrioxamine: a new bifunctional chelate for facile radiolabeling of monoclonal antibodies with zirconium-89 for immuno-PET imaging. Eur. J. Nucl. Med. Mol. Imaging 37, 250–259. https://doi.org/10.1007/s00259-009-1263-1.

Peynshaert, K., Devoldere, J., Minnaert, A.-K., De Smedt, S.C., Remaut, K., 2019. Morphology and Composition of the Inner Limiting Membrane: Species-Specific Variations and Relevance toward Drug Delivery Research. Curr. Eye Res. 44, 465–475. https://doi.org/10.1080/02713683.2019.1565890.

The Principles of Humane Experimental Technique, 1960. . Med. J. Aust. 1, 500–500. https://doi.org/10.5694/j.1326-5377.1960.tb73127.x.

Rafic Hariri University Hospital, 2011. The Safety and Tolerability of Intravitreal Adalimumab in Patients With Refractory Diabetic Macular Retinopathy or Choroidal Neovascularization or Uveitis: A Pilot Study (Clinical trial registration No. NCT00855608). clinicaltrials.gov.

Robertson, M., Liversidge, J., Forrester, J.V., Dick, A.D., 2003. Neutralizing tumor necrosis factor-alpha activity suppresses activation of infiltrating macrophages in experimental autoimmune uveoretinitis. Invest. Ophthalmol. Vis. Sci. 44, 3034–3041. https://doi.org/10.1167/iovs.02-1156.

Ryman, J.T., Meibohm, B., 2017. Pharmacokinetics of Monoclonal Antibodies. CPT Pharmacomet. Syst. Pharmacol. 6, 576–588. https://doi.org/10.1002/psp4.12224.

Sadeghi, A., Puranen, J., Ruponen, M., Valtari, A., Subrizi, A., Ranta, V.-P., Toropainen, E., Urtti, A., 2021. Pharmacokinetics of intravitreal macromolecules: Scaling between rats and rabbits. Eur. J. Pharm. Sci. Off. J. Eur. Fed. Pharm. Sci. 159, 105720 https://doi.org/10.1016/j.ejps.2021.105720.

Sánchez-López, E., Espina, M., Doktorovova, S., Souto, E.B., García, M.L., 2017. Lipid nanoparticles (SLN, NLC): Overcoming the anatomical and physiological barriers of the eye - Part I - barriers and determining factors in ocular delivery. Eur. J. Pharm. Biopharm. Off. J. Arbeitsgemeinschaft Pharm. Verfahrenstechnik EV 110, 70–75. https://doi.org/10.1016/j.ejpb.2016.10.009.

Santos Lacomba, M., Marcos Martín, C., Gallardo Galera, J.M., Gómez Vidal, M.A., Collantes Estévez, E., Ramírez Chamond, R., Omar, M., 2001. Aqueous humor and serum tumor necrosis factor-alpha in clinical uveitis. Ophthalmic Res. 33, 251–255. https://doi.org/10.1159/000055677.

Schmitt, M., Hippeläinen, E., Raviña, M., Arango-Gonzalez, B., Antopolsky, M., Vellonen, K.-S., Airaksinen, A.J., Urtti, A., 2019. Intravitreal Pharmacokinetics in Mice: SPECT/CT Imaging and Scaling to Rabbits and Humans. Mol. Pharm. 16, 4399–4404. https://doi.org/10.1021/acs.molpharmaceut.9b00679.

Sha, O., Kwong, W.H., 2006. Postnatal Developmental Changes of Vitreous and Lens Volumes in Sprague-Dawley Rats. Neuroembryology Aging 4, 183–188. https://doi.org/10.1159/000118928.

Shahab, M.A., Mir, T.A., Zafar, S., 2019. Optimising drug therapy for non-infectious uveitis. Int. Ophthalmol. 39, 1633–1650. https://doi.org/10.1007/s10792-018-0984-1.

Suami, H., Scaglioni, M.F., 2017. Lymphatic Territories (Lymphosomes) in the Rat: an Anatomical Study for Future Lymphatic Research. Plast. Reconstr. Surg. 140, 945–951. https://doi.org/10.1097/PRS.0000000000003776.

Sugita, S., Takase, H., Taguchi, C., Mochizuki, M., 2007. The role of soluble TNF receptors for TNF-alpha in uveitis. Invest. Ophthalmol. Vis. Sci. 48, 3246–3252. https://doi.org/10.1167/iovs.06-1444.

The Association for Research in Vision and Ophthalmology- Statement for the Use of Animals in Ophthalmic and Vision Research [WWW Document], n.d. URL http

s://www.arvo.org/About/policies/statement-for-the-use-of-animals-in-ophthalmic-and-vision-research/ (accessed 1.17.22).
Tsirouki, T., Dastiridou, A., Symeonidis, C., Tounakaki, O., Brazitikou, I., Kalogeropoulos, C., Androudi, S., 2018. A Focus on the Epidemiology of Uveitis. Ocul. Immunol. Inflamm. 26, 2–16. https://doi.org/10.1080/09273948.2016.1196713.
Varela-Fernández, R., Díaz-Tomé, V., Luaces-Rodríguez, A., Conde-Penedo, A., García-Otero, X., Luzardo-Álvarez, A., Fernández-Ferreiro, A., Otero-Espinar, F.J., 2020. Drug Delivery to the Posterior Segment of the Eye: biopharmaceutic and pharmacokinetic considerations. Pharmaceutics 12, E269. https://doi.org/10.3390/pharmaceutics12030269.
Verel, I., Visser, G.W.M., Boellaard, R., Stigter-van Walsum, M., Snow, G.B., van Dongen, G.A.M.S., 2003. 89Zr immuno-PET: comprehensive procedures for the production of 89Zr-labeled monoclonal antibodies. J. Nucl. Med. Off. Publ. Soc. Nucl. Med. 44, 1271–1281.
Waldmann, T.A., Strober, W., 1969. Metabolism of immunoglobulins. Prog. Allergy 13, 1–110. https://doi.org/10.1159/000385919.